Log Number: 194

AN EXPERIMENTAL STUDY ON THE IDENTIFICATION OF FLOW PATTERNS RESPONSIBLE FOR CROSSFLOW IN A VERTICAL TUBE BUNDLE GEOMETRY

A. Mahmood¹, M. Rohde¹, T. H. J. J. vander Hagen¹, R. F. Mudde¹ and T. Ikeno²

Delft University of Technology, Delft, The Netherlands

² Nuclear Fuel Industries Ltd., Osaka, Japan

 $\underline{samasl@yahoo.com, \, \underline{m.rohde@tudelft.nl}, \, \underline{t.h.j.j.vanderhagen@tudelft.nl}, \, \underline{r.f.mudde@tudelft.nl}, \, \underline{t-ikeno@nfi.co.jp}}$

Abstract

The aim of the present study is to enhance the current understanding of crossflow in a vertical tube bundle geometry in an experimental way. LDA measurements were carried out in a 4 x 4 tube bundle having diameter to pitch ratio of 0.7 for Reynolds numbers ranging approximately from 600 to 11,000. Water was used as a working fluid at isothermal, single-phase flow and ambient operating conditions. The experimental results showed the existence of large-scale coherent structures for laminar, transitional and turbulent flows. The secondary flow patterns were resolved as well. A comparison of the root mean square of cross velocity fluctuations in the gap region, being a measure of cross-flow, with the magnitude of the secondary flows reveals a dominant contribution of the former over the latter. Furthermore, the successful use of FEP in the above-mentioned experiments as solid, refractive index matching material in water has been demonstrated.

1. Introduction

In vertically aligned rod bundles, such as the ones in the cores of PWR's and BWR's, many researchers have identified the existence of lateral flow (crossflow) due to large-scale coherent structures and secondary flows. These lateral flows contribute to the exchange of heat and voids between the sub-channels in such a reactor bundle (i.e. cross-flow mixing). The underlying physical mechanisms and the contribution of these large-scale coherent structures and secondary flows towards cross-flow mixing, however, is still an issue debated in the scientific community.

Earlier attempts to explain the flow characteristics in a rod bundle were concentrated mainly on the Reynolds stress driven secondary flows. Skinner et al. [1] were the first who attributed the higher rate of diffusivity in the gap to secondary flow since the mixing rates they measured were higher than could be accounted for by turbulent diffusion alone. Later, following the ideas of Skinner et al. [1] Singh and Pierre [2], Trupp and Azad [3] and Vonka [4, 5] emphasized the role of secondary flows in inter-sub-channel scalar transport.

In 1973-1974, Rowe et al. [6, 7] published their two component LDA measurements in rod bundles arranged in a square array. Their results clearly show that there exists an additional macroscopic flow process in the regions adjacent to the gaps, resulting in periodic flow pulsations across the gaps. The macroscopic flow pulsations observed by Rowe [6] have been confirmed by Hooper, Rehme and Wood [8, 9, 10, 11].

In 1991, Möller [12] investigated the macroscopic flow pulsations a 4-rod facility (previously used by Rehme) as a function of gap width and channel Reynolds number with the help of hot

wire anemometry. He proposed a flow model of a street of vortices moving in the center of the gap rotating alternately in opposite direction. The macroscopic flow pulsations, caused by such large-scale vortices, cover almost the full cross-section of the sub-channel.

The present experimental study is intended to look into the near gap mean flow properties and behaviour of coherent vortices in a tube bundle geometry for a large range of Reynolds numbers, an aspect missing in most of the previous studies. Another aim of this study is to investigate the contribution of secondary flows to crossflow in a tube bundle geometry. The non-intrusive experimental technique, Laser Doppler Anemometry (LDA), has been used for the flow field measurements. The use of LDA allows study of flow field free from any measuring probe effect (associated with intrusive measurement techniques).

2. Laser Doppler Anemometry (LDA)

The non-intrusive point measurement optical LDA technique is based on determining the frequency shift that light waves undergo when scattered by moving particles, i.e. the Doppler shift. Detailed information on LDA can be found in e.g., Durst et al. [13] and Tummers [14]. The velocity data for the present study was obtained with a two-component LDA setup. The laser used was a water cooled Ar-laser (by Spectra-Physics-Stabilite 2016) with a maximum power of 4.0 W. The laser light was separated into different wavelengths (λ_i), i.e., colored pairs of laser beams, using a TSI Colorburst 9201, with one beam of each pair shifted in frequency by the acousto-optic modulator, a Bragg cell. For the present study, two wavelengths were used, i.e., the blue pair ($\lambda_b = 488.0$ nm) for the streamwise velocity component and the green pair ($\lambda_g = 514.5$ nm) for the flow in the spanwise direction, see Figure 1.

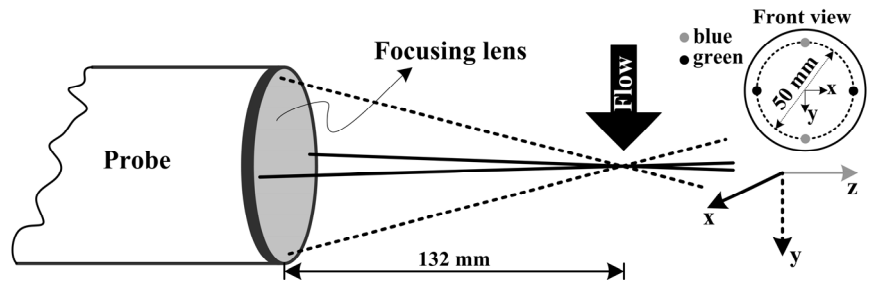


Figure 1 LDA probe setup for two components measurement, used in the present study. The focal length of the probe-focusing lens is 132.0 mm. The system of coordinates used for the measurements is also shown.

The seeding particles used have a diameter of 8-12 ($x10^{-6}$) m, a density of 1.05 - 1.15 kg/m³ and a refractive index of 1.5. The maximum amount of seeding during the experiment did not exceed 10^{-4} % of the volume of fluid, assuring that the fluid properties remained unchanged by this small amount of the seeding particles.

Dantec Dynamics BSA flow software and MatLab were used for online and offline data handling/processing, respectively. The BSA flow software also controlled the probe traversing system. Post processing of the velocity time series, received from the BSA flow software, was carried out by using in-house software for the following corrections/tasks:

Removal of the velocity bias

Log Number: 194

- Implementation of coincidence criteria
- Checking for multiple validation
- Application of a slotting technique for the determination of the autocorrelation function and auto power spectral density (APSD).

For details of these LDA data treatments see [14, 15, 16].

3. Refractive index matching (RIM)

One of the disadvantages of LDA is the requirement of optical access to the measurement region. The use of transparent, solid and curved/skewed walls, having a refractive index mismatched fluid around them, poses problems due to the refraction of the light beams. A solution to this problem is to match the refractive indices (η) of the fluid and the solid transparent walls, i.e., to make the latter optically "disappear" in the former. For the present study, with water as the working fluid, Fluorinated Ethylene Propylene (FEP) was selected as the solid material. At 20.0 °C, the refractive index of FEP ($\eta \approx 1.338$) is very close to the refractive index of water ($\eta \approx 1.333$). Furthermore, the applicability of FEP as a RIM material was checked by comparing the results of velocity measurements for a turbulent flow in a FEP pipe with reference data [17].

4. Tube bundle setup and experimental flow loop

Figure 2 shows the tube bundle test section in flow loop and the LDA measurement section. The spanwise, streamwise and the transverse directions are represented by x, y, and z coordinates, respectively. The corresponding x, y and z-velocity components are u, v and w, respectively. Looking at the cross sectional view, the test section consists of eight near wall and one central sub-channels formed by setup of 4×4 tubes (4 quarter tubes, 8 half tubes and 4 full tubes). The diameter (D) to pitch (P) ratio in most of LWR fuel assemblies ranges from 0.77 to 0.70. The D/P of the tubes in the current setup had been chosen to be 0.7, for comparison reasons with the numerical work of Ikeno and Kajishima [18]. The tubes have a 25.0 mm outer diameter and a wall thickness of 0.25 mm that fulfills the data rate criteria [17]. Two separate centrifugal pumps lead water from the reservoir tank to overflow vessels A and B. Vessel A was meant to feed the main flow through the test section and vessel B was used to over-pressurize (and thus strengthen) the thin FEP tubes in the measurement section. The flow in the test section was gravity driven and had 4.0 m of developing length (\approx 100 times the cross sectional hydraulic diameter) before it entered the measurement section.

Flow straightening, i.e., removal of any swirl and cross stream movement of the fluid, was achieved by placing a honeycomb structure of 60.0 mm height and a mesh size of 6.0 mm at the inlet of the test section. The fluid flow was regulated by a set of valves and rotameters located between the outlet of the test section and the water reservoir tank. Figure 2 also shows the cross sectional view of different segments of the test section. The test section casing upstream and downstream of the measurement section consisted of 4 and 2 segments, each of length 1.0 m, respectively. The measurement section had a length of 0.14 m with a casing made of Perspex to facilitate the LDA optics. The half and the quarter tubes in path of the laser beams were shaped from 0.25 mm thick FEP sheet, whereas, the others were made from PVC rods. Flanges joined all the pieces of the test section casings as smooth as possible. Each of four central tubes consisted of three parts in the streamwise direction; PVC tubes in the upstream and downstream

section and a steel pipe in between with an optical access window located at the height of the measurement section.

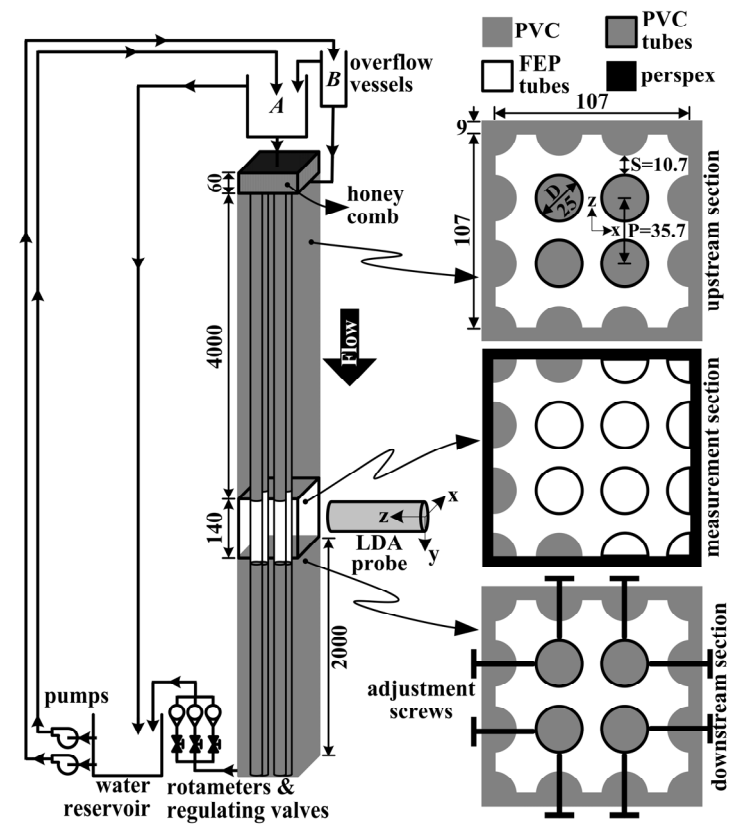


Figure 2 Experimental flow loop used for LDA measurements in a tube bundle. The figure also shows the cross sectional view of three segments of the test section along with the system of coordinates used. All dimensions are in mm and the figure is not to scale.

The optical access window in a pipe was made first by cutting out a part of steel pipe and then covering the opening with a 0.25 mm thick heat shrinkable FEP sleeve. This setting resulted in firm, vertically aligned FEP tubes with the drawback that some regions of the measurement section became inaccessible for LDA measurements. However, by optimally positioning the intact steel portions of the optical access windows, the central sub-channel region remained fully accessible for LDA measurements, as shown in Figure 3 (a).

Grids were placed at all flanges, except the one joining the measurement and the upstream section, to restrict the lateral movement of the four central tubes hanging from the top of the test section. Placement and smoothness of the grid ensured that the measurement section remains free from wake disturbances of the grid structure.

To determine the four central tubes position, LDA measurements for laminar flow were performed along lines defining the gaps minimum spacing (S). A parabola fitted to laminar measurements and extrapolated to zero velocity near the tube walls gave an accurate estimate of tube positions. Adjustment screws located just downstream of the measurement section (see Figure 2) were used to fine-tune the four central tubes positions. The maximum error in the tube positions was found to be ± 0.8 mm, which is 7.5% of minimum gap spacing S.

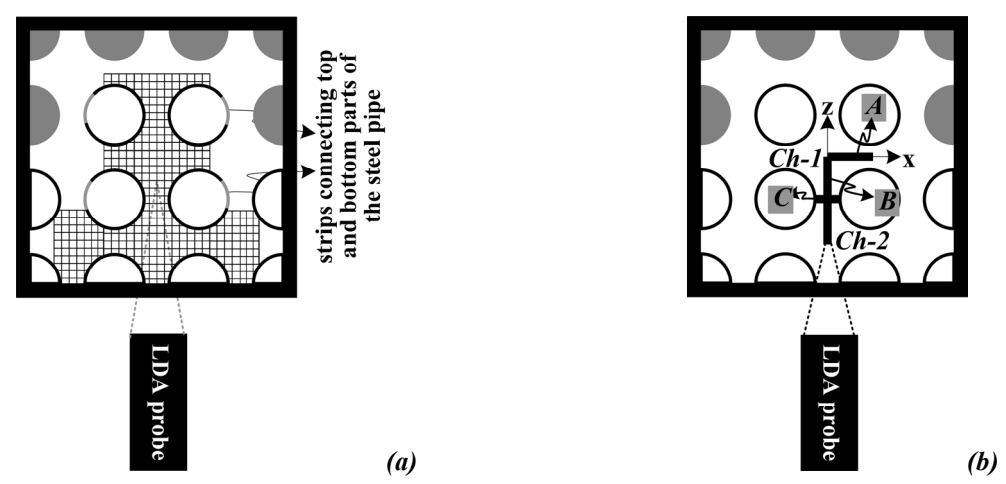


Figure 3 (a) Cross sectional view of the tube bundle setup depicting the region accessible for LDA measurements (highlighted by a checker pattern). (b) LDA measurement lines A, B and C. Center and near-wall sub-channels are identified as Ch-1 and Ch-2, respectively.

5. Experimental results

This section presents the LDA results depicting the mean flow properties and the flow patterns in the tube bundle geometry under consideration. Being a representative of the actual sub-channel in a tube bundle geometry, the target region for the present study was the central sub-channel. The results presented in this section are for channel Reynolds numbers (Re_{ch}) ranging from 631 to 11037. Re_{ch} is based on the total cross-sectional hydraulic diameter and the bulk velocity (V_{bulk}). The upper limit was based on the maximum flow possible. The measurements were carried out along three straight lines A, B and C, see Figure 3 (b). Line A, located at z=0.0 and extending from x=0.0 to x=P/2, covers half of the gap region and half of the central sub-channels. Line B, located at x=0.0, extends from z=0.0 to z=P and covers the full gap region and half of the adjacent sub-channels. Line C at z=P/2 extends from x=±S/2 and covers the minimum gap spacing. The center and near wall sub-channels covered by the line B are designated as Ch-1 and Ch-2, respectively.

5.1 Time averaged streamwise velocity profiles

Figure 4(a) shows examples of four streamwise velocity profiles measured along lines B and C normalized by the V_{bulk} . The unsymmetrical behavior of the profile along line B is due to the presence of the outer casing wall near Ch-2. The streamwise velocity profile along the line C clearly identifies whether the flow in the gap region is laminar or turbulent. For Re_{ch} =631 and 1419, the flow in the gap region is laminar, confirmed by fitting a parabolic curve to the measurements. At Re_{ch} =3153, a transition from laminar to turbulent flow in the gap is depicted by the results. At Re_{ch} =11037 a fully turbulent streamwise velocity profile in the gap region is visible.

To estimate the flow type in the gap region from Re_{ch} , a plot of the approximate gap Reynolds numbers (Re_{g-app}) vs. the channel Reynolds number (Re_{ch}) can be used, see Figure 4(b). Re_{g-app} is based on the gap hydraulic diameter (D^h_{gap}) and the streamwise velocity averaged in time and space between $z=\pm D/2$ along the line B, i.e., the gap region. Therefore, the real gap Reynolds numbers calculated from the streamwise velocity based on the total cross sectional gap region flow area (between $z=\pm D/2$) would be somewhat higher than the Re_{g-app} . Assuming a Reynolds

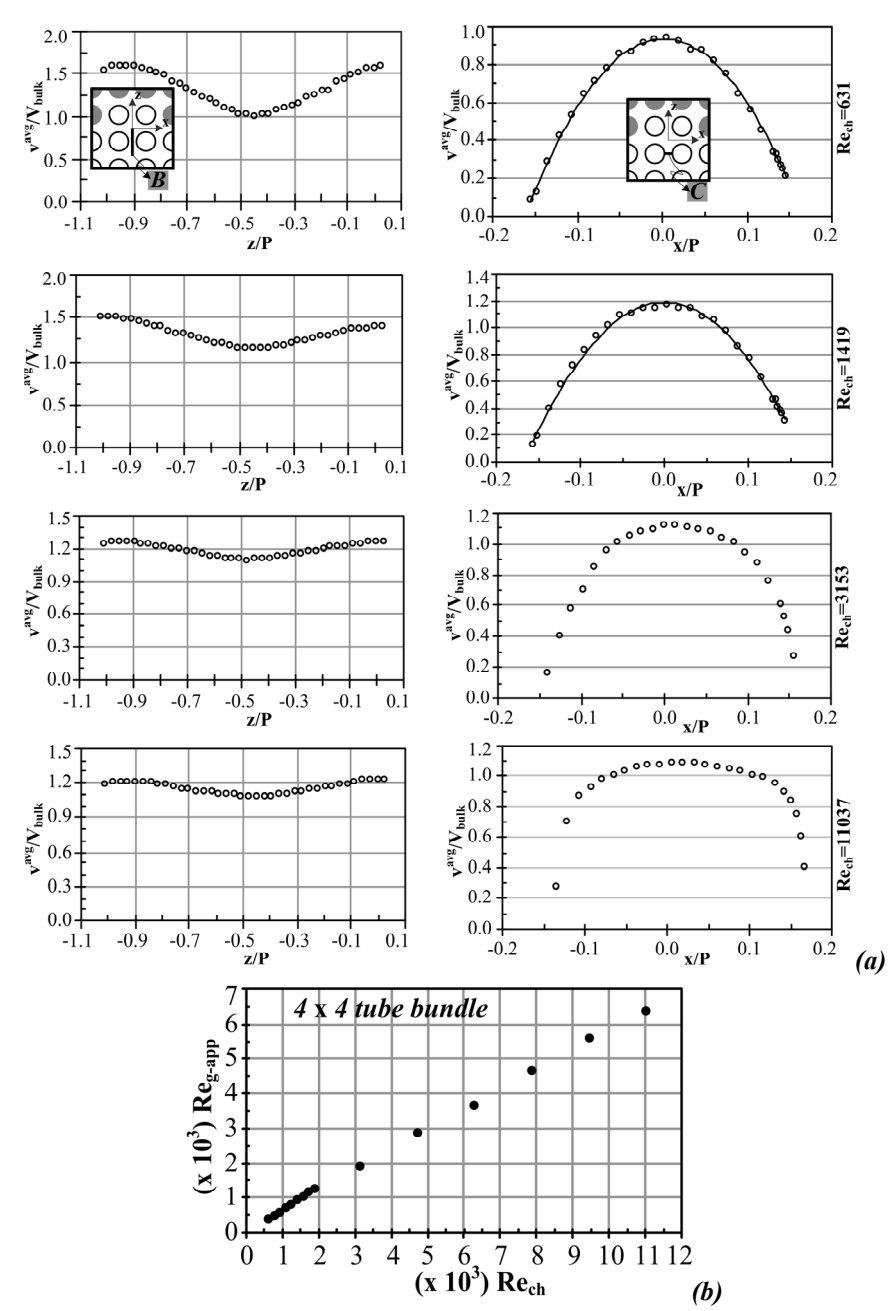


Figure 4 (a) Streamwise velocity profiles along line B (1st column) and line C (2nd column). Line B and C are shown as insets in top figures. The distances and velocities are normalized by the pitch (P) and the *V_{bulk}, respectively. (b) Approximate gap Reynolds numbers as a function of channel Reynolds numbers.

number of 2000 roughly as an upper limit for the existence of laminar flow, the flow in the gap region is laminar up to $Re_{ch}\approx 3200$. Figure 5 shows locations of the inflection points (being indicative of the boundary between the channel's high flow and gap's low flow regions), maxima and minima on the streamwise averaged velocity profile. The location of the inflection point falls within a band of $z/P=\pm 0.05$. The asymmetric distribution of these points is due to the combined effect of the gap shape and the outer casing wall on the streamwise velocity profile.

 $^{^*}$ V_{bulk} = (total flow rate) / (the lateral cross sectional flow area of the tube bundle).

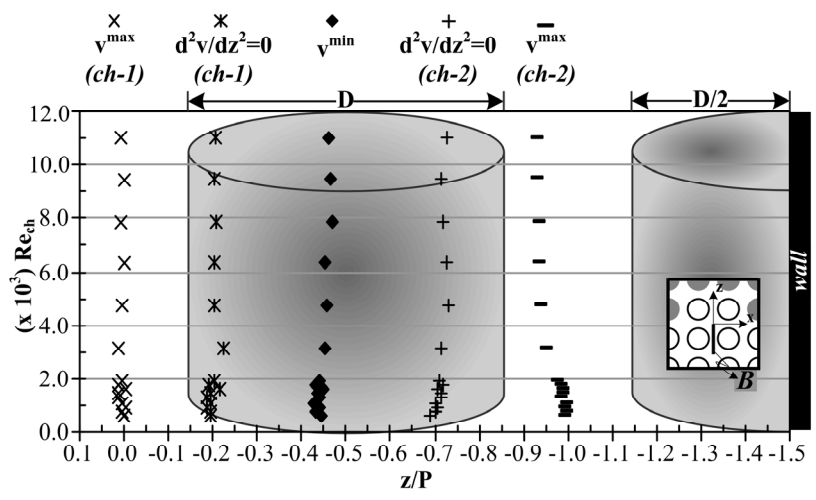


Figure 5 Location of points of maxima, minima and inflection on the time-averaged streamwise velocity profile measured along line B in the tube bundle.

5.2 Dependence of flow characteristics on Re_{ch}

Figure 6 (a) shows the magnitude of the time averaged velocities at the points of maxima (v^{max}), minima (v^{min}) and inflection ($v^{inflec.pt.}$) as a function of Re_{ch}. Figure 6 (a) also shows the average of v^{max} and v^{min} (v^{avg}).

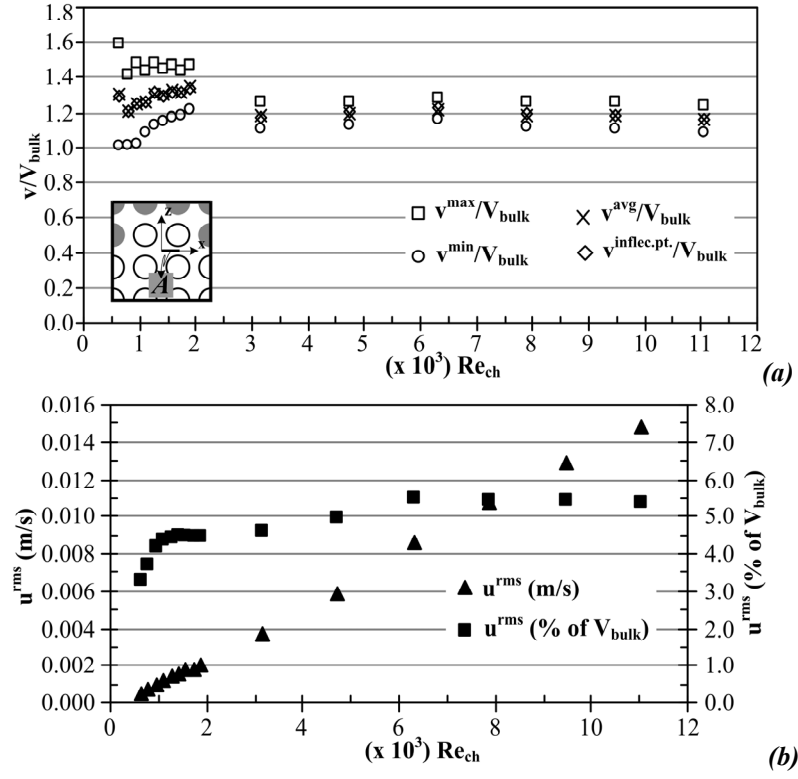


Figure 6 (a) Normalized magnitude of velocities at points of maxima, minima and inflection on the streamwise velocity profile as a function of Re_{ch} measured along line A. (b) A comparison between the absolute and normalized RMS of the spanwise velocity fluctuations in the gap region as a function of Re_{ch} . The u^{rms} of the velocity signal measured at (x/P, y/P, z/P)=(0.5, 0.0, 0.0) is presented.

All values of velocities are non-dimensionalized by V_{bulk} . For $Re_{ch}>3000$ (marking the transition from laminar to turbulent flow in the gap region) all the velocities linearly scale with the V_{bulk} (and thus with Re_{ch}). For all Re_{ch} , v^{max} is practically the sub-channels center line velocity (v^{CL}), free from any near wall effect, and hence scales linearly with V_{bulk} .

The root mean square of the spanwise velocity fluctuations (u^{rms}) in the gap region, a measure of crossflow, is shown in Figure 6 (b). The measurements were performed along line A (see Figure 4). All values of u^{rms} are presented in absolute values and as a percentage of V_{bulk} . Clarification of this figure requires knowledge on the coherent structures in the bundle geometry. Therefore, the coherent structures need to be investigated first, which will be done in the next section.

5.3 Coherent structures

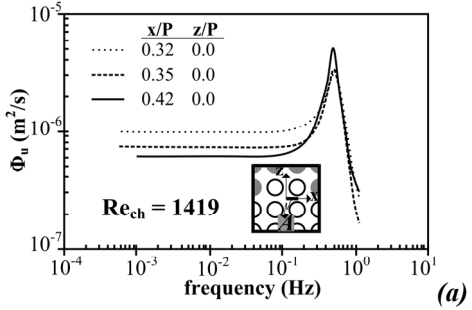
The streamwise size of the near gap coherent vortices was estimated from Taylor's frozen flow hypothesis by using Equation (1), i.e.:

$$L^{str} = v^{str} \cdot t \tag{1}$$

where L^{str} = the streamwise length of the vortex

 v^{str} = the streamwise structure velocity

t = coherent vortices characteristic time scale.



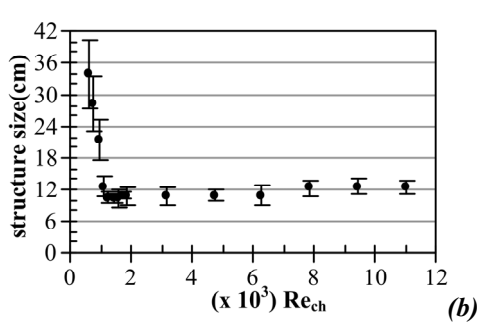


Figure 7 (a) An example of APSD of the cross velocity component measured along the line A at locations (x/P=0.32, z/P=0.0), (x/P=0.35, z/P=0.0) and (x/P=0.42, z/P=0.0) for Re_{ch}=1419. Peaks in the plot indicate the presence of coherent vortices. (b) Structure size in cm as a function of Re_{ch}.

With LDA, being a single point measurement technique, it is not possible to obtain v^{str} by using a two point cross correlation. Based on the results of compound channels [19], it is assumed that in the tube bundle $v^{str} \approx v^{inflec.pt.}$. From compound channels results the $v^{inflec.pt.}$ is expected to differ from v^{str} by \pm 7.0 % (for $Re_{ch} \ge 4000$) and \pm 30.0 % (for $Re_{ch} < 4000$). The presence of coherent vortices appears as a peak in the one-dimensional auto power spectral density (APSD) plot [20] of a cross velocity time signal measured at a point in the flow field, as shown in Figure 7 (a). The time scale t in Equation (1) is estimated from the frequency of the peak in the APSD plot of the gap spanwise velocity signal. Figure 7 (b) depicts the streamwise structure size estimated from Equation (1), averaged along the x-axis (line A) at 10 measurement points as a function of Re_{ch} .

Main conclusions drawn from above mentioned results are:

- comparing Figures 6 (b) and 7 (b), for Re_{ch} < 2000 low and high values of u^{rms} are associated with relatively large and small structure sizes, respectively;
- for Re_{ch} > 2000, in contrast to coherent vortices found in a free shear flow, the structure size becomes independent of flow properties probably due to the wall bounded shear flow effect.

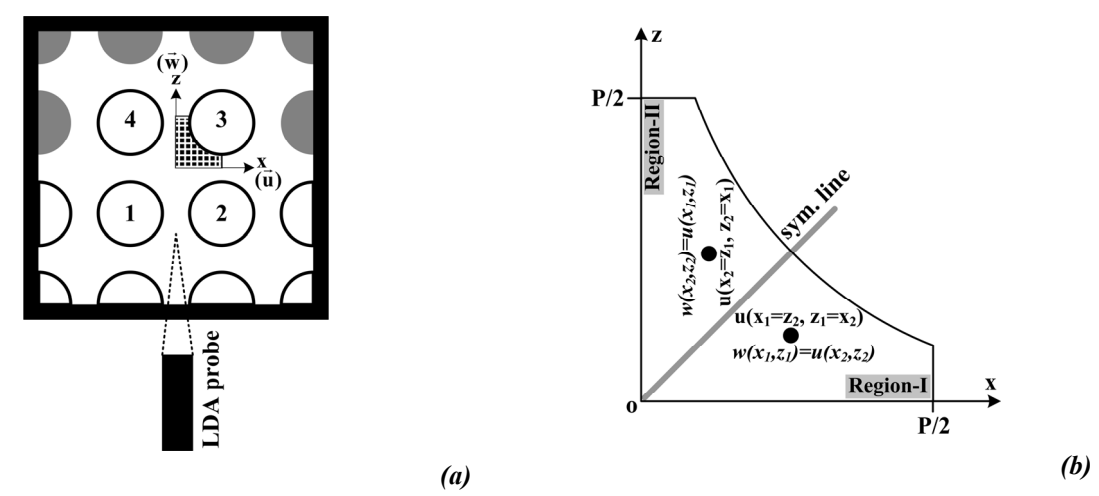


Figure 8 (a) Secondary flows measurement region in xz-plane, (b) Estimation of the transverse velocity component (w) from the measured spanwise component (u) using the symmetry line.

6. Secondary flows

This section presents the results of measurements carried out to investigate secondary flows at Re_{ch}=9130 in the tube bundle geometry. The aim is to find out whether in a tube bundle the large-scale structures contribution towards the crossflow dominates over the secondary flows or not. LDA measurements were performed in a quarter of the central sub-channel on a grid with dx=dz=1.0 mm within the flow area bounded between x/P=z/P=0.0 to x/P=z/P=0.5, see Figure 8 (a). The experimental findings presented in this section are compared with CFD simulation (LES) results of Ikeno and Kajishima [18]. The simulation domain size used was $6P\times2P\times2P$ in the streamwise, spanwise and transverse directions with periodic boundary conditions in all directions. The 2D-LDA measurement gives only the spanwise velocity component (u) in the xz plane. An estimate of secondary flows on the other hand also requires the transverse velocity component (w). To estimate w, the u measured at a point in Region-I was projected across the symmetry line to obtain w at a point (equidistant from the symmetry line) in Region-II and vice versa, see Figure 8 (b).

From Figure 9, showing the numerical and experimental secondary flow results in the form of vectors and stream traces plots, it can be deduced that:

- secondary flow patterns are resolved by using the LDA measurements;
- ignoring the spurious vectors at $x/P=z/P\approx0.5$, the maximum magnitude of the measured secondary flow vector is found to be 0.9% of the maximum average streamwise velocity at the origin (vmax). This value is higher than the 0.7% found in the CFD results.

Figure 10 depicts a quantitative comparison in the form of the mean spanwise velocity profiles at different transverse, z/P, positions (the grey lines in Figure 9(a) and (c)). Although a qualitative agreement with the simulations is present, most of the measured values are on the higher side compared to the reference CFD results. The maximum spanwise velocity component reported in the CFD results is nearly 0.5% of the V_{bulk} . It is very difficult to measure such small velocities keeping in view the following factors contributing to the uncertainties in the measurements:

- instrumentation noise;
- attenuation of the laser beams by the FEP resulting in a weaker LDA signal;
- reflection of laser light from FEP surface, decreasing the validation of the LDA burst;
- the measurement volume misalignment that could be caused by a misaligned LDA probe and/or a refractive index mismatch (although small in our case) between FEP and water.

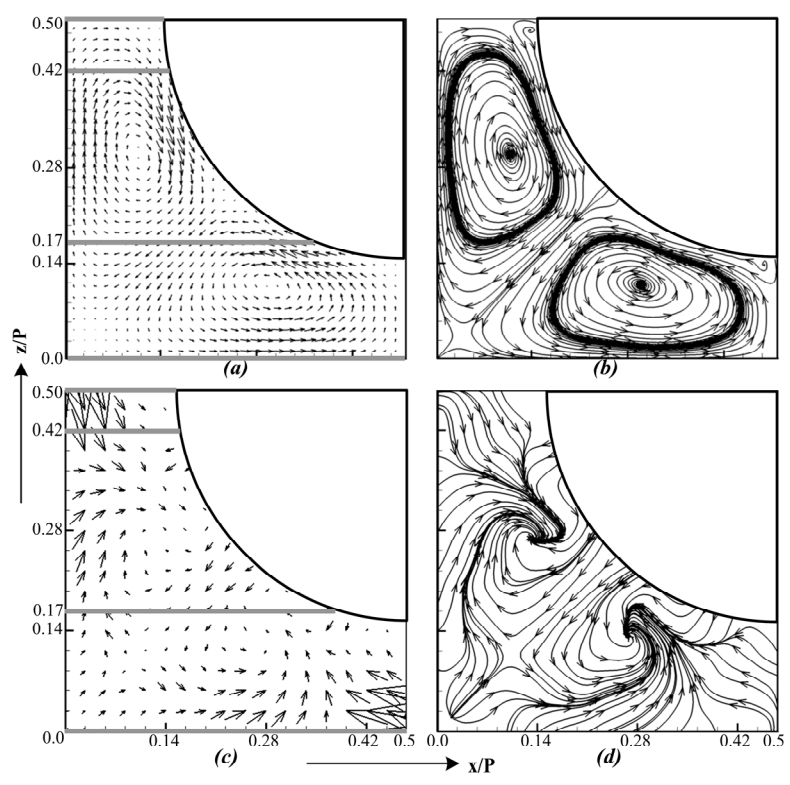


Figure 9 Secondary flow vectors from (a) CFD [18] and (c) LDA measurements. Plot of the stream traces for (b) CFD [18] and (d) LDA measurements. Re_{ch}=9130.

The spurious vectors in Figure 9, located near $x/P=z/P\approx0.5$, are due to the noisy LDA signal resulting from passage of the incident and reflected laser beams through multiple layers of FEP, as mentioned above. In addition to these factors, the differences in the CFD and experimental results might also be due to the following dissimilarities between the simulation and the experimental setup:

- geometric irregularities in the experimental setup, particularly due to the thin walled water filled FEP tubes in the measurement section;
- asymmetry in the central sub-channel of the experimental facility due to an error in the four central tubes positioning;
- as mentioned earlier, the CFD results were obtained for an infinitely long and wide tube bundle geometry, where a periodic boundary condition in each direction were used [18]. The walls, located in the spanwise and the transverse directions (at x/P=z/P=1.5), possibly have an influence on the experimental results.

By comparing the magnitudes of the measured secondary flows (\approx 0.9% of v^{max}) and the u^{rms} (\approx 5.0% of V_{bulk}) in the gap region (shown in Figure 6(b)) it might be concluded that the coherent structures contribute to the crossflow mixing for the larger part.

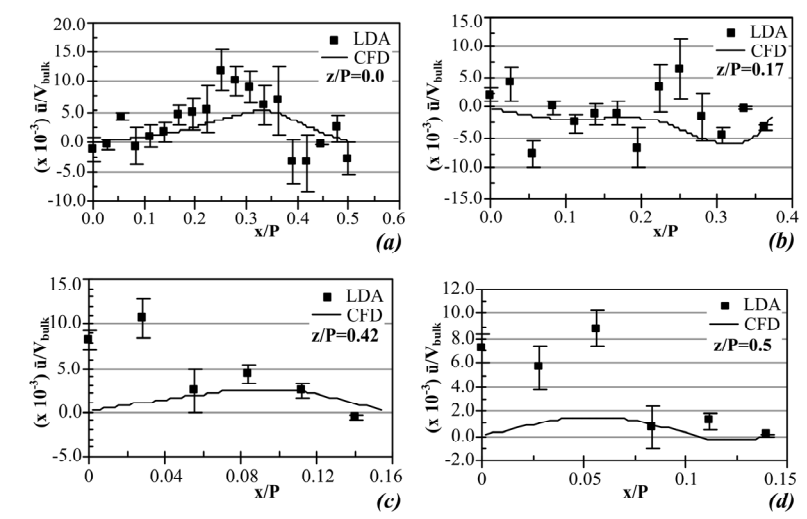


Figure 10 Mean spanwise velocity profiles at Rech=9130 along the lines at (a) z/P=0.0, (b) z/P=0.17, (c) z/P=0.42 and (d) z/P=0.5. Rech=9130.

7. Conclusions

The velocity field in the gap region of a 4x4 vertical tube bundle has been studied. The focus of the study was to investigate the crossflow through the gap region resulting from different flow patterns. Experiments have been performed using the 2D-LDA technique for channel Reynolds numbers ranging from 631 to 11037. The conclusions that can be drawn from the study are as follows:

- The bundle geometry shows a typical mixing-layer streamwise velocity profile a prerequisite for inducing the coherent structures.
- The tube bundle gap geometry allows a large expansion of channel fluid flowing towards the middle of the gap. This effect is expected to be beneficial for mixing.
- Qualitatively, secondary flows were successfully identified in the sub-channel of a tube bundle geometry. However, due to very small magnitudes of the spanwise velocity component and the high noise level in the LDA velocity signal, a quantitative agreement with CFD results was not achieved. Nevertheless, the measured secondary flow, being 0.9% of the v^{max} , is even lower than the spanwise velocity fluctuations in the gap region (\approx 5.0% of V_{bulk}). This shows a minor role of secondary flows toward the inter-sub-channel crossflow and presumably less important in crossflow mixing also.

8. References

- [1] Skinner, V., R., Freeman, A., R., Lyall, H., G., "Gas mixing in rod clusters", Int. J. Heat Mass Transfer, 12(1969), pp. 265-278.
- [2] Singh, K., Pierre, St., C., C., "Single phase turbulent mixing in simulated rod bundle geometries", Trans. CSME, 1(1972), pp. 73-80.
- [3] Trup, A., C., Azad, R., S., "The structure of turbulent flow in triangular array rod bundles", Nucl. Eng. Des., 32(1975), pp. 47-84.
- [4] Vonka, V., "Measurement of secondary flow vortices in a rod bundle", Nucl. Eng. Des., 106(1988), pp. 191-207.

- [5] Vonka, V., "Turbulent transports by secondary flow vortices in a rod bundle", Nucl. Eng. Des., 106(1988), pp. 209-220.
- [6] Rowe, D. S., "Measurement of turbulent velocity, Intensity and scale in rod bundle flow channels", PhD.-Thesis, Oregon State University, BNWL-1736, Battelle Pacific Northwest Laboratories, Richland, Washington (1973).
- [7] Rowe, D. S., Johnson, B. M., Knudsen, J. G., "Implications concerning rod bundle crossflow mixing based on measurements of turbulent flow structure", Int. J. Heat Mass Transfer, 17(1974), pp. 407-419.
- [8] Rehme, K., "The structure of turbulent flow through a wall subchannel of a rod bundle", Nucl. Eng. Des., 45(1978), pp. 311-323.
- [9] Hooper, J. D., "Developed single phase turbulent flow through a square-pitch rod cluster", Nucl. Eng. Des., 60(1980), pp. 365-379.
- [10] Hooper, J. D., Rehme, K., "Large-scale structural effects in developed turbulent flow through closely-spaced rod arrays", J. Fluid Mech., 145(1984), pp. 305-337.
- [11] Hooper, J. D., Wood, D. H., "Fully developed rod bundle flow over a large range of Reynolds number", Nucl. Eng. Des., 83(1984),pp. 31-46.
- [12] Möller, S.V., "On phenomena of turbulent flow through rod bundles", Exp. Thermal Fluid Sci., 4 (1991), pp. 25-35.
- [13] Durst, F., Melling, A., Whitelaw, J., H., "Principles and Practice of Laser Doppler Anemometry", 2nd ed., 1981, Academic Press, London.]
- [14] Tummers, M., J., "Investigation of a turbulent wake in an adverse pressure gradient using laser Doppler anemometry", PhD thesis, 1999, Delft University of Technology, The Netherlands.
- [15] Benedict, L., H., Nobach, H., Tropea, C., "Estimation of turbulent velocity spectra from laser Doppler data", Meas. Sci. Technol., 11(2000), pp. 1089-1104.
- [16] Nobach, H., "Local time estimation for the slotted correlation function of randomly sampled LDA data", Exp. Fluids, 32(2002), pp. 337–345.
- [17] van Campen, L.J.A.M., Mahmood, A., Rohde, M., Portela, L.M., "An Experimental Study on the Capabilities of FEP as Refractive Index Matching Material for LDA: Turbulent Pipe Flow", The 7th International Topical Meeting on Nuclear Reactor Thermal Hydraulics, Operation and Safety (NUTHOS-7), Seoul, Korea Oct. 2008
- [18] Ikeno, T., Kajishima, T., "Analysis of dynamical flow structure in a square arrayed rod bundle", Nucl. Eng. Des., 240(2010), pp. 305-312.
- [19] Lexmond, A. S., Mudde, R. F., van der Hagen, T., "Visualization of the vortex street and characterization of the cross flow in the gap between two sub-channels", NURETH-11, Avignon, France, Oct. 2-6, (2005).
- [20] Bonnet, J., P., Delville, J., Glauser, M., N., Antonia, R., A., Bisset, D., K., Cole, D., R., Fiedler, H., E., Garem, J., H., Hilberg, D., Jeong, J., Kevlahan, N., K., R., Ukeiley, L., S., Vincendeau, E., "Collaborative testing of eddy structure identification methods in free turbulent shear flows", Exp. Fluids, 25(1998), pp. 197–225.